Springer

KSME

Journal of Mechanical Science and Technology 27 (6) (2013) 1~7
www.springerlink.com/content/1738-494x
DOI 10.1007/s12206-011-0913-y

Purge flow effect on aerodynamics performance in high-pressure turbine cascade †

W Ghopa Wan Aizon[1,2], Ken-ichi Funazaki[1] and Takemitsu Miura[1]

[1]*Department of Mechanical System Engineering, University of Iwate, Morioka, 020-8551, Iwate, Japan*
[2]*Department of Mechanic and Materials, Faculty of Engineering, National University of Malaysia, Bangi, Malaysia*

(Manuscript Received 000 00, 2013; Revised 000 00, 2013; Accepted 000 00, 2013)

Abstract

The endwall and blade film cooling systems are the typical solution adopted within gas turbines to allow further increase of turbine inlet temperature, avoiding critical material thermal stresses. Due to the complex secondary flow field in the blade passage, endwall is more difficult to be cooled than blade surfaces. In the matter of fact, in endwall film cooling studies, it is necessary to investigate the interaction between coolant air and the secondary flow. In present study, the flow field of high-pressure turbine in linear cascade has been investigated by 5-holes pitot tube to reveal the secondary flows behaviour under the influenced of purge flows through a slot which is located $0.63C_{ax}$ upstream of blade leading edge. Both measurement and numerical simulation presented almost similar trend of aerodynamics performance thus more accurate secondary flow structures can be revealed by the prediction. The presence of newly generated vortical structures was considered to be responsible to the additional loss at higher MFR cases.

Keywords: Purge flow; Upstream leakage; Endwall film cooling; Aerodynamics performance; Secondary flow; Total pressure loss

1. Introduction

In general, continuous increase of turbine inlet temperature will improve the overall performance of a gas turbine. Most of the modern gas turbines are operating at turbine inlet temperature of 1800 K. Such high temperature has been made possible by the enhancement of the thermal protection applied on turbine components; nozzles, blades, and combustion wall. One of the critical regions that require special thermal protection intention is the endwall. This region is considerably difficult to be cooled due to complex secondary flow structure that occurs at the blade passage. The endwall flow structure has been revealed by Takeshi et. al [1]. The main flow structure consists of pressure side and suction side leg horse-shoe vortex, cross flow, corner vortex and passage vortex. The earliest study that relates the endwall flow structure and film cooling has been made by Blair [2]. The work clarifies that, the horse-shoe vortex and passage vortex has a dominant impact on the heat transfer of film-cooled endwall. Due to the existence of complex flow structures in this region, detail studies are required in order to improve the cooling performance. Several studies have presented the flow field data within the vane stagnation plane illustrating the formation and dynamics of the leading edge horse-shoe vortex which include the works of Goldstein and Spores [3], Langston et. al [4], Sieverding [5] and Wang et. al [6]. Studies by Kang et al. [7] and Radomsky and Thole [8] revealed the effect of inlet Reynolds number and turbulence level respectively on the formation of the horse-shoe vortex. Both studies were not included the purge flows. Using the same cascade of the previous study [7, 8], Sundaram and Thole [9] performed LDV measurements to reveals the effect of the purge flow on the endwall flow structure to enable direct comparison with the previous result [7, 8]. In the actual application, purge flow is the coolant which by passed from the compressor and injected through the combustor/stator or stator/rotor rim seal for endwall surface protecting purpose. Rehder and Dannhauer [10], has carried out the experiments to reveal the effects of injection flow angle from the upstream clearance of linear cascade of LPT stator vanes. The observation shows that the leakage ejection perpendicular to the main flow direction amplifies the secondary flow, in particular the horse-shoe vortex and therefore increases the secondary losses near the endwall region, whereas tangential leakage ejection causes significant reduction of horse-shoe vortex and at the same time decreasing the secondary losses at the cascade exit. Recently, Thrift and Thole [11] investigated the effects of orientation and position of the purge flow. The observations show a dramatic difference in horse-shoe vortex formation at the stagnation plane which is directly influenced by the orientation and position of the purge flow. Studies on various test conditions are required to have detailed information on related study. Based on above mentioned literatures, it

*Corresponding author. Tel.: +81196216422, Fax.: +81196216422
E-mail address: wanaizon@gmail.com
† Recommended by Associate Editor

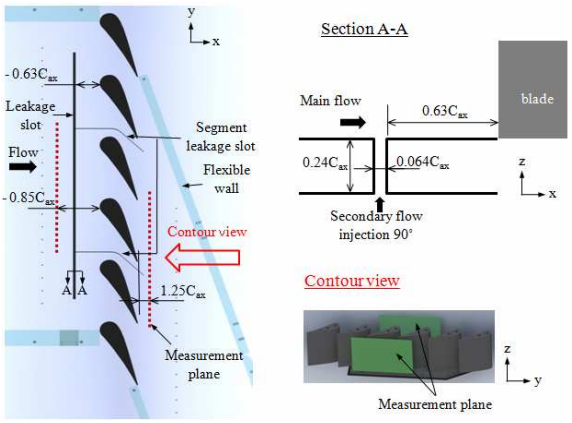

Fig. 1. Measurement area and slot geometry.

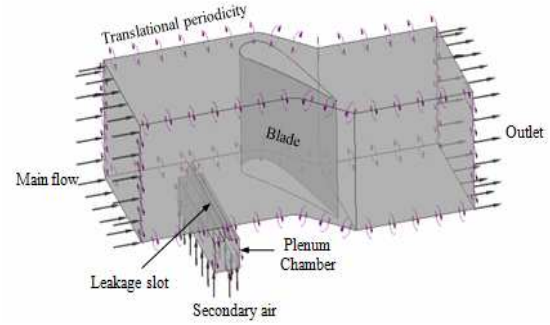

Fig. 2. Geometry of the CFD model.

is clear that cooling air injection from upstream slot highly influenced the aerodynamics performance of turbine cascade. Furthermore, slot location and geometry as well as cooling air amount need to be carefully considered to achieve the optimum setting. In present works, a new model with slightly lower solidity and higher aspect ratio compared with previous test blade [12] has been designed. The slot location also was moved away from the blade leading edge. The study focuses on the aerodynamics effect of purge flow on the secondary flow field. The coolant was ejected from the slot located upstream of blade leading edge. Aerodynamic measurements were performed by the use of pneumatic 5-hole pitot tube to measure a total pressure at blade downstream. The numerical simulation was also conducted for the validation and to predict the interaction of ejected coolant with the main flow.

2. Experimental procedures

The experimental investigations were conducted in the aero-engine laboratory at Iwate University. Measurement plane and slot geometry are shown in Fig. 1. The leakage slot was located $0.63C_{ax}$ upstream of the blade leading edge. The slot extended about 4 pitches and the width was $0.064C_{ax}$ (4 mm). In consideration of the plate thickness, normal injection into the main flow was highly expected in this study. All components of the test section except the test cascade were made of acrylic-resin plate in order to keep the visibility from outside. The test cascade consisted of 2 segments, each of which had two identical HP turbine nozzle vanes, and two dummy vanes. The vane segments were produced by a rapid prototyping method using UV light hardening technique. L-type miniature pitot tube was placed upstream of the model leading edge for inlet flow velocity measurement. The measurement system is constituted by pneumatic 5-holes Pitot tube, traverse device, pressure transducer and data logger which are connected to the computer for data collection. 5-hole pitot tube were traversed at $1.25C_{ax}$ downstream of blade leading edge to measure total pressure and three dimensional flow velocity. The location of traverse plane and the viewpoint definition of all contours are also shown in Fig. 1. In present study, various ejection amount represented by MFR starting from 0.75% up to 2.24% were tested to observe their effect on the endwall flow structure. However, the measurement without any leakage was firstly carried out to observe a baseline condition of flow field at blade downstream plane. For baseline condition case, a measurement was conducted without supplying a secondary air, therefore a flat endwall platform without slot was placed at the first to avoid a flow that coming from the high pressure main stream moving into the slot. The measurements at downstream plane were done by two phases where the first phase was to investigate a periodicity of flow at cascade outlet. 1200 points of measurement were started from the blade tip which traversing for 2 pitches and ended close to the endwall. Then, second phase measurement were surveyed with a finer grid for only 1 pitch and a measurement started at midspan. The finest grid was 1 mm and coarsest was 10 mm with a 1120 points of measurement. Furthermore, the finer grid was adopted near the region where the blade wakes are expected. This plane has been surveyed by means of 28 traverses in the pitchwise direction. Each of them constituted by 40 measuring points spaced with variable steps which have a finer grid near the endwall. For each measuring point, 10 samples have been collected and the pressures were calculated as time-averaged components. However, results based on finer grid measurements only will be presented in this paper. The head diameter of probe was 2.1 mm and the nearest distance of measurement from the endwall was 2 mm. The main flows Reynolds number of 1.25×10^5 was fixed throughout all test cases. This Reynolds number was determined based on blade chord length.

3. Computational procedures

As illustrated by Fig. 2, the computational domain for the study of the three dimensional upstream leakage flow in linear cascade flow consisted of the plenum, 1 pitch endwall with a single blade periodicity channel designed by slot located upstream the vane. The computational mesh system was created using Gridgen (Pointwise) to generate a fully structured meshes. This is a multiblocks meshing method which consisted of 10 structured blocks. The density of mesh cells is

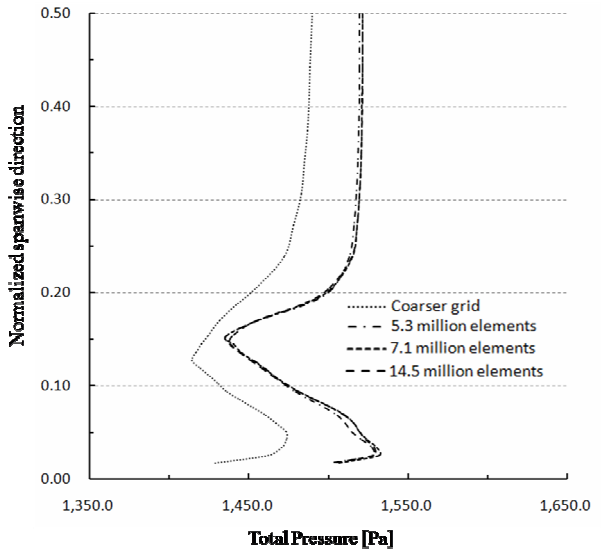

Fig. 3. Grid dependency test.

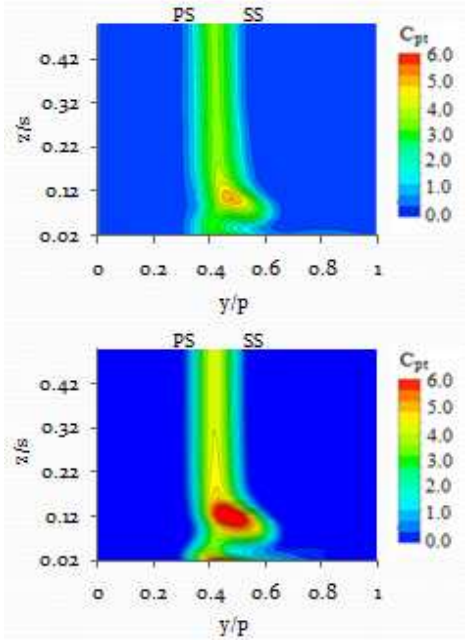

Fig. 4. Total pressure loss for baseline condition based on EFD(top) and CFD(bottom).

increased in the vicinity of the bottom, the top and the blade surfaces but also at injection location. The height of wall-adjacent cells in these regions is 0.02 mm with the objective to obtain y+ value close to 1 along the walls. The entire computational domain comprises a total of 7.1 million of hexahedral cells. To evaluate the grid independence of the solution, meshes have been tested with a coarser, 5.3 million, and 14.5 million of elements. Fig. 3 indicated the spanwise direction of total pressure near the blade downstream to explain the grid number used in this study (7.1 million elements) was quite enough for the flow prediction. The change of the total pressure almost cannot be seen compared to the finest grid with 14.5 million elements. A numerical prediction was adopted by commercial software, ANSYS CFX 12. A very popular SST turbulence model were employed in this study in order to observe the performance of those models in predicting the secondary flow field under the influence of purge flow. Domain extended from $2.0C_{ax}$ upstream of the leading edge to $2.0C_{ax}$ downstream of the trailing edge. The boundary conditions are defined in accordance with the measurement conditions for each case. Translational periodic boundary condition was applied on the pitchwise direction. Uniform distributions of measured stagnation pressure and static temperature were specified on the main inlet boundary. As for the secondary flow, the measured mass flow rate and static temperature were specified on the entry plane of the plenum chamber. Non-slip and adiabatic conditions were given on the wall surface.

4. Uncertainty analysis

Uncertainty associated with the pneumatic measurement was mostly governed by the accuracy of the pressure transducers. The accurate pressure transducer with ±0.5 [Pa] was used for these cases. A method of estimating uncertainty in experimental results has been presented by Kline and McClintock [13]. Uncertainties were estimated using the partial derivative and root-sum-square method. Based on procedure, the uncertainty of the inlet velocity was approximately ±1.7% and the uncertainty associated with the loss coefficient for the airfoil wake centre was about ±4.9%. The relative errors for MFR measurement were calculated based on pitot tube and the laminar flow meter. Relative error of MFR resulted to be 2.6%, 1.7%, 2.1% and 4.1% for MFR of 0.8%, 1.2%, 1.68% and 2.24%, respectively. For CFD, by considering the cost and CPU time required, other factors which contribute to the uncertainties in the simulation has been neglected except for the grid number as shown in the previous section (Fig. 3). The calculated relative error of the predicted total pressure loss coefficient based on grid number of 7.1 million and 14.5 million elements is approximately 1.6%.

5. Results and discussions

5.1 Baseline performance

Fig. 4 presents the total pressure loss coefficients contours at blade downstream plane for the baseline condition. The top figure represents the C_{pt} contour measured by the experiment and the bottom figure represents the C_{pt} contour predicted by the CFD. The results show the contributed losses by the wake profile which occurs along the span direction. In addition, the contours also characterized by the presence of the passage vortex represented by the high loss core approximately at y/p=0.48 and z/s=0.1. Although the numerical result shows relatively the same location of the loss core, the numerical simulation has over predicted the losses value. This is might

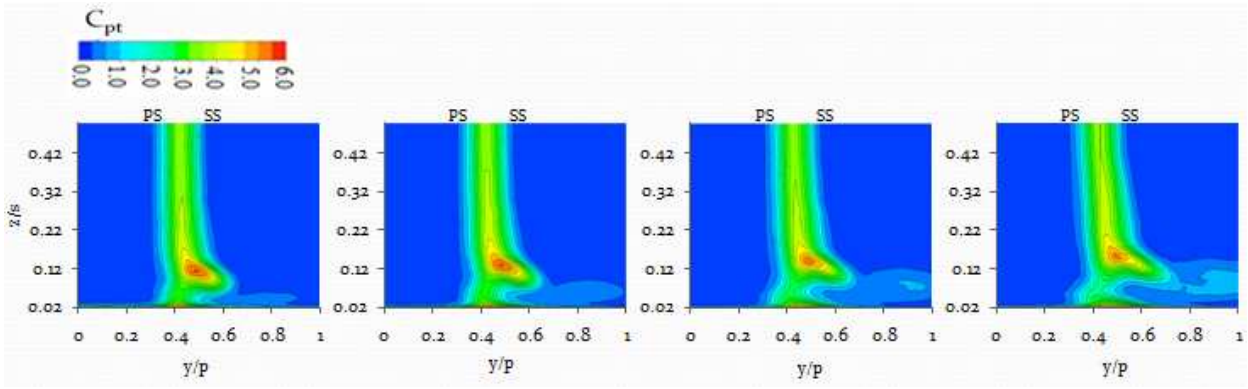

MFR=0.75% MFR=1.2%

Fig. 5. Total pressure loss contours for each case based on EFD.

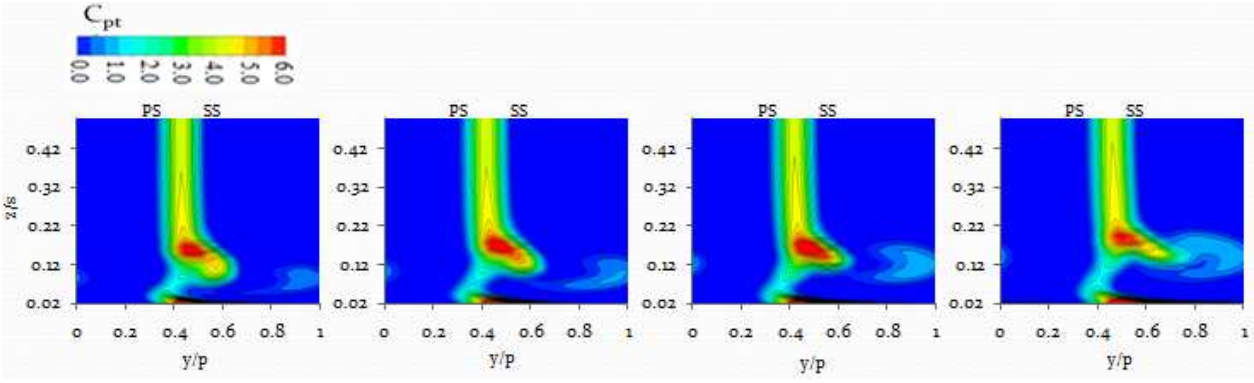

MFR=0.75% MFR=1.2%

Fig. 6. Total pressure loss contours for each case based on CFD.

be due to the different of inlet profile used in the prediction compared to the measurement. The CFD result also show an additional loss core close to the endwall located at y/p=0.42. The loss core represents the loss contributed by the corner vortex which commonly occurs at the near wall region. This loss core cannot be observed in the experimental result as shown in Fig. 4. The nonexistent of the loss core in the experimental result is due to the limitation of the present measurement devices and the accessibility of the near wall region.

5.2 Purge air injection effects on aerodynamics performance

Fig. 5 and Fig. 6 show the C_{pt} contour on the blade downstream plane at different MFR value captured by the experiments (EFD) and the numerical simulations (CFD), respectively. Four different mass flow ratios, MFR have been considered at 0.75%, 1.20%, 1.68% and 2.24%. These MFR represent lower, immediate, high, and extremely high purge injection cases, respectively. The discussion will first focuses on the EFD results in Fig. 5. The figure indicates that the upstream leakage ejection has a significant influence on the secondary flow structures across the MFR value. In comparison to the baseline case, the loss core associated with the passage vortex can be observed to occur further away from the wall corresponding to the MFR values. At MFR = 0.75%, additional loss region can be observed to occurs at the endwall region covering the pitch distance from y/p=0.6 up to y/p=0.6. As the MFR increases, the additional loss region also increases as shown by the contour of MFR=1.2%, 1.68% and 2.24%. At high purge ejection case, MFR=1.68%, an additional loss core can be observed at y/p=0.9. Furthermore, high MFR also cause deformation on the shape of the loss core characterized by the passage vortex. Both of the phenomena become more apparent at MFR=2.24%. The introduction of purge flow at blade upstream increases the endwall vortical structures strength, consequently contributes to the additional losses. The CFD results show similar trends as the EFD. Fig. 6 shows the occurrence of the additional losses and deformation of the initial loss region associated with the increase of MFR. Similar to the EFD, the position of the loss core predicted by CFD can be observed to move away from the wall as the MFR increases. Although the similar trend can be observed, the CFD results show slight discrepancy in terms of the shape and location of the loss core. The discrepancy could be contributed

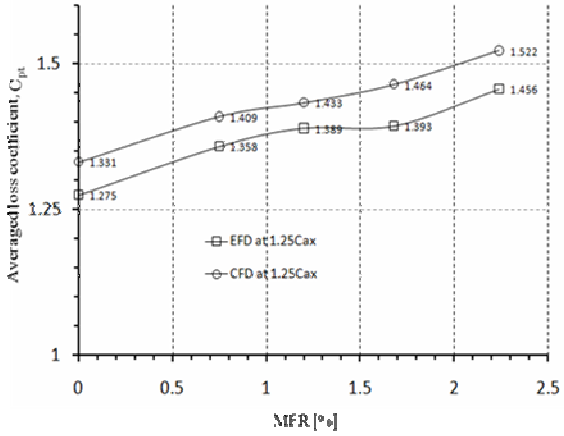

Fig. 7. Plane averaged total pressure loss, C_{pt}.

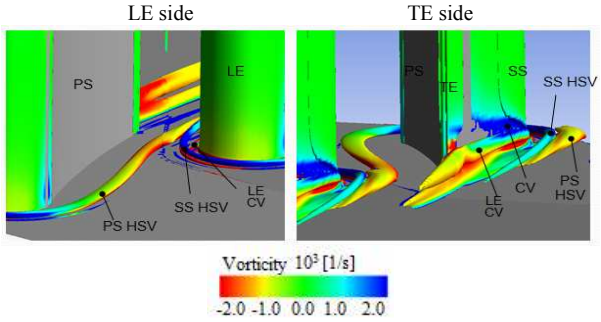

(a) Baseline Condition

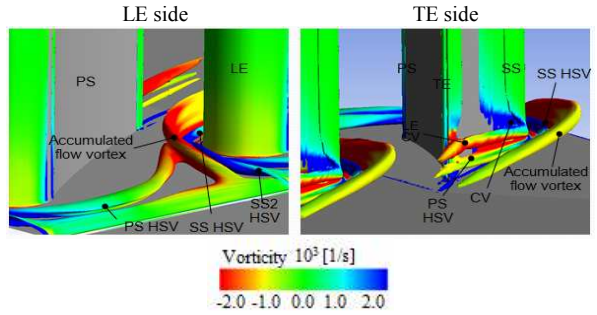

(b) MFR=1.2%

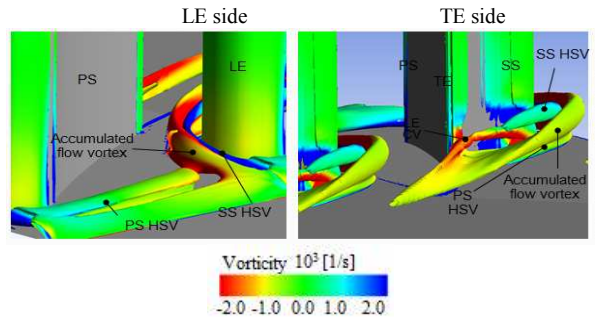

(c) MFR=2.24%

Fig. 8. Vortex core on endwall region.

by the different inlet flow profile used in the CFD which influence the development of the passage vortex. With regard to the loss region characterized by the corner vortex which has been observed earlier (Fig. 6), wider loss region can be observed at higher MFR which indicates the increase of the corner vortex strength. Fig. 7 shows the plane average total pressure loss for all the cases involved in the present study. The contribution of the MFR towards the aerodynamic loss can directly specify from the graph. A similar pattern can be observed between the EFD and CFD results. Based on EFD, the loss has increased approximately at 6.5% for MFR=0.75% and further increased up to 14.2% for MFR=2.24% in comparison to the baseline case. Having the similar trends, the losses predicted by the CFD also increased 5.8% and 14.3% for the MFR=0.75% and 2.24%, respectively. In general, the graph shows that CFD is over predict the losses in the range of 3%~5% in comparison to EFD.

5.3 Predicted flow structures

Based on the good agreement that have been achieved between the EFD and CFD, the present section intended to provide details flow structures on the endwall region predicted by the CFD. The details will provide futher understanding on the interaction between the coolant and the main flow. Fig. 8(a), (b) and (c) show the vortex core generated at the swirling strength equal to 760 [s^{-1}] for baseline condition, MFR=1.2% and MFR=2.24%, respectively. The color of the vortex core is representing the vorticity, ζ valued within the range of 2000 [s^{-1}] and –2000 [s^{-1}]. To obtain the full understanding on the vortex propagations, each figure illustrates the generated vortex core near blade leading edge and trailing edge. In the baseline case, CFD has predicted the formation of pressure side leg horse-shoe vortex (PS HSV) and suction side leg horse-shoe vortex (SS HSV) near the blade leading edge. The presence of the leading edge corner vortex (LE CV) has also be predicted at both sides of blade leading edge with a smaller core compared to HSV. Further downstream of the blade leading edge, it can be observed that PS HSV was deflected by the SS HSV before attaching onto the adjacent blade SS surface. This SS HSV actually coming from adjacent blade suction.

HSV actually coming from adjacent blade SS and losing its swirling energy when travels away from the blade leading edge. In contrast, the strength of the LE CV increases at the blade throat and developed in the same direction with the PS HSV to become a large passage vortex at blade downstream plane. The loss core which was presented in Fig. 5 and 6 are considered to be associated with this particular vortex core. The figure also shown the origin of the counter vortex (CV). At MFR=1.2%, a newly generated vortex core clearly can be observed along the pitch direction just downstream of the slot. Due to the high pressure near the blade stagnation region, the ejected coolant tends to move towards centre of the blade passage and accumulated with the opposite flow direction of the coolant coming from adjacent blade.

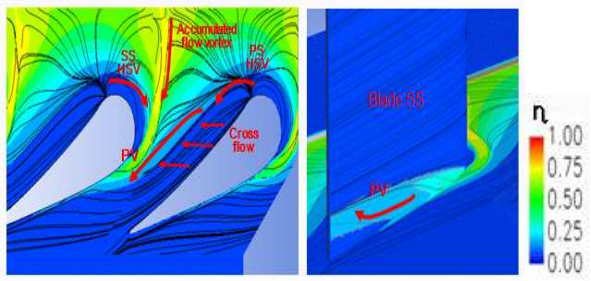

(a) Endwall (b) Blade SS

Fig. 9. Film cooling effectiveness on endwall (a) and blade SS (b) by CFD.

This phenomenon has influenced to the formation of new vortex core (accumulated flow vortex) which then developed along the blade SS surface. As shown in Fig. 5 and 6, the presence of this vortex core might be responsible to the additional loss which was generated after the coolant ejection. At MFR=2.24%, ejected coolant has much higher momentum to penetrates into the main stream; particularly near the stagnation region compared to the lower MFR cases. The penetration provides the blockage to the mainstream thus affecting the formation and strength of HSV. Figure clearly explained the increase of HSV strength with the higher swirling energy of the core compared to the baseline case. As the MFR increases, the HSV strength is also increases. This result in increase of PS HSV energy which will allow it to travel across from blade PS and attach onto adjacent blade SS. Noted that the higher energy provided to the PS HSV, the earlier the reattachment onto the adjacent blade SS occurs. This phenomenon will consequently deflected the direction of the LE CV upwards. The explanation parallel to the position of loss core which is shifted towards midspan at a higher MFR as shown in Fig. 5 and 6. Some of the ejected coolant acting like HSV vortex near blade leading edge (SS2 HSV) which then merged with the SS HSV near the blade throat as shown by the case of MFR=1.25%. Based on figure, the generation of the passage vortex at blade downstream for the baseline case is actually the combination of LE CV and the PS HSV. The larger passage vortex that were observed for the MFR cases is associated to the accumulated flow vortex core coming from upstream.

5.4 Effects of flow behaviour on film cooling effectiveness

Fig. 9 shows the influence of the secondary flow structures on endwall film cooling distribution. The figure illustrates the prediction of film cooling effectiveness on the endwall region (a) as well as blade SS surface (b) at MFR=1.2% together with the endwall streamline. As shown in the figure, cooling coverage provided by the purge flow was highly influenced by the secondary flows structures on the endwall region which was discussed in previous section. The presence of the PS HSV and SS HSV near the blade leading edge leave the area unprotected. The contour shows that higher cooling effectiveness was observed at the region where the coolant flow was accumulated. Furthermore, the cross flow and movement of the passage vortex (PV) from blade PS to blade SS provide a wider cooling coverage near the adjacent blade SS instead of blade PS. The merging of PS HSV and LE CV to generate a larger PV along the blade SS surface enable the coolant to provide a lower film cooling effectiveness trail as shown on the right figure.

6. Conclusions

The investigation of aerodynamics performance on turbine cascade with endwall cooling by the influenced of purge flow has been done by 5-hole pitot tube measurement and numerical simulation. They represent almost similar trend of performance and enable authors to take advantage of numerical simulation to accurately predict the interaction of ejected coolant with the main flow. Based on the results obtained, the following conclusions can be drawn:

- Purge flow has significantly affected the secondary flow fields. The presence of the additional losses near the blade SS was captured even for a lower case ejection of 0.75%. Based on tested MFR, this loss region expanded approximately 40%-50% of area. MFR=2.24% was contributed to the highest loss among others. The newly generated vortical structures have been captured by the CFD with a higher swirling strength travel along the blade SS, which consequently contributed to the additional losses
- The loss core which was indicated in the baseline case was also affected by the purge ejection. Measurement showed that the position of the core induced by the passage vortex slightly moved towards midspan for any increases of MFR with approximately 15%, 28%, 38% and 55%, respectively, compared to the baseline case. Injecting the coolant from upstream was predicted to amplify the strength of PS HSV so that it deflected the direction of LE CV to move upwards thus providing a slightly higher position of loss core for the higher MFR case.
- The overall total pressure loss was proportional to the MFR and the graph plotted enable the authors to estimate the loss providing with another case of MFR. CFD over predicted the loss approximately 3% to 5% compared to the measurement.
- The flow behaviour on the endwall region was also highly influenced the coolant, providing the cooling protection area.

The modification of the approaching flow caused by the purge flow has a strong influence on the development of downstream flow structures thus required detailed experimental investigation near the slot downstream to enhance the understanding of the interaction of the purge flow into the main stream.

Acknowledgements

The authors are grateful acknowledgement to Hitachi Ltd. , Japan for the financial support in this study.

Nomenclature

C : Chord length (0.0122 m)
C_{ax} : Axial chord length of blade (0.0623 m)
Q : Volume flow rate
m : Mass flow rate
U_{in} : Inlet velocity
U_z : Axial velocity
ρ : Density
n : Number of pitch
P_s : Static pressure
P_d : Dynamic pressure
P_{ti} : Inlet total pressure
P_{to} : Outlet total pressure
A : Duct section area
p : Cascade pitch
s : Blade span height
y : Picthwise direction
z : Spanwise direction
SS : Suction surface
PS : Pressure surface
T_{aw} : Adiabatic wall temperature [˚C]
T_∞ : Main flow temperature [˚C]
T_2 : Secondary air temperature[˚C]

Subscript

∞ : Main flow
2 : Secondary air

Abbreviation

MFR : Mass flow ratio = $(\rho Q)_2/(\rho Q)_\infty$
C_{pt} : Total pressure loss coefficient=$(P_{ti}- P_{to})/(1/2)\ \rho\ U_{in}^2$
η : Film cooling effectiveness=$(T_{aw} - T_\infty)/(T_2- T_\infty)$

References

[1] K. Takeishi, M. Matsuura, S. Aoki and T. Sato, An experimental study of heat transfer and film cooling on low aspect ratio turbine nozzles, ASME Paper No. 89-GT-187, ASME Journal of Turbomachinery, 112 (1990) 488-496.
[2] M. F. Blair, An experimental study of heat transfer and film cooling on large-scale turbine endwalls, ASME Journal of Heat Transfer, 96 (1974) 524-529.
[3] R. J. Goldstein and R. A. Spores, Turbulent trans port on the endwall in the region between adjacent turbine blades, ASME Journal of Heat Transfer, 110 (1988) 862-869.
[4] L. S. Langston, M. L. Nice and R. M. Hooper, Three-dimensional flow within a turbine cascade passage, ASME Paper No. 76-GT-50, ASME Journal of Engineering for Power, 99 (1977) 21-28.
[5] C. H. Sieverding, Recent progress in the understanding of basic aspects of secondary flows in turbine blade passages, ASME Paper No. 84-GT-78, ASME Journal of Engineering for Gas Turbines and Power, 107 (1984) 248-257.
[6] H. P. Wang, S. J. Olson, R. J.Goldstein and E. R. Eckert, Flow visualisation in a linear turbine cascade of high performance turbine blades, ASME Paper No. 95-GT-7, Houston, Texas (1995).
[7] M. B. Kang and K. A. Thole, Flowfield measurements in theendwall region of a stator vane, ASME Paper No. 99-GT-188, ASME Journal of Turbomachinery, 122 (1999) 255-262.
[8] R. W. Radomsky and K. A. Thole, High frees tream turbulence effects on endwall heat transfer for a gas turbine stator vane, 122 (2000) 699-708.
[9] N. Sundaram and K. A. Thole, Film-cooling flow fields with trenched holes on an endwall, J. of Turbomachinery, 131 (2009).
[10] H. J. Rehder and A. Dannhauer, Experimental investigation of turbine leakage flows on the three-dimensional flow field and endwall heat transfer, Journal of Turbomach, 129 (2007) 608-618
[11] A. A. Thrift, K. A. Thole and S. Hada, Effects of orientation and position of the combustor-turbine interface on the cooling of a vane endwall, ASME 2011, GT2011-455 (2011).
[12] W. G. Aizon and K. Funazaki, Aero-thermal performance of purge flow in turbine cascade endwall cooling, Applied Mechanics and Material, 229-231 (2012) 737-741.
[13] S. J. Kline and F. A. McClintock, Describing uncertainties in single sample experiments, Mechanical Engineering, 75 (1953) 3-8.